

## Analysis of evaporative cooling in street canyons: coupled model and advanced imaging of transport in porous media

S. Saneinejad<sup>1,2</sup>, T. Defraeye<sup>3</sup>, B. Blocken<sup>4</sup>, P. Moonen<sup>2</sup>, D. Derome<sup>2</sup> and J. Carmeliet<sup>1,2</sup>

<sup>1</sup>Chair of Building Physics  
 ETH Zürich, 8093 Hönggerberg, Switzerland

<sup>2</sup>Laboratory of Building Science and Technology  
 Empa, 8600 Dübendorf, Switzerland

<sup>3</sup>CVCBT/MeBioS, Department of Biosystems,  
 Katholieke Universiteit Leuven, 3001 Heverlee, Belgium

<sup>4</sup>Building Physics and Services  
 Eindhoven University of Technology, 5600 Eindhoven, The Netherlands

### Abstract

Urban heat islands affect the energy use for cooling in an urban environment, as well as human comfort and health. Water evaporation from moist surfaces could potentially reduce the local temperature in urban areas, a process known as evaporative cooling. In this paper, a coupled model is employed to study the effect of evaporative cooling on the temperature conditions in an urban street canyon. Neutron radiography images are used to validate the model.

### Introduction

A heat island is an urban area which can be several degrees warmer than its surrounding rural hinterland. The temperature difference is higher during the night and when winds are weak (Santamouris, 2001). The urban heat island affects the energy use for cooling in an urban environment, as well as human comfort and health. One way to mitigate the excess heat is to make use of evaporative cooling, for example from ground-level ponds and roof ponds, from surfaces wetted by wind driven rain or from vegetated surfaces.

In this paper, a coupled model is used to investigate how the local wind flow pattern induces non-uniform drying of the urban surfaces, and how this drying results in a modification of the local micro-climate and the thermal comfort in the street canyon. The model takes into account the influence of direct short-wave radiation, long-wave radiative exchange between the surfaces and the sky (including multiple reflections), effect of latent heat of evaporation, detailed material properties and buoyancy. For validation, using neutron radiography, an experiment documents the drying of porous materials exposed to a controlled air flow in a micro wind tunnel.

### Coupled model

We propose a coupled model to simulate the drying process of a wet porous surface in an urban environment. The coupled model consists of three sub-models: a CFD model which solves the convective heat, air and moisture transport in the air, a Building Envelope Heat and Moisture (BE-HAM) model which solves the heat and moisture transport within the porous material, and a radiation model (RAD) which solves the radiative balance for short-wave and long-wave radiative exchange between the building surfaces and the sky. An important aspect of this model is the accurate modeling of the exchange of the convective heat

and mass fluxes at the interface between the air and the porous domain. Since for long street canyons exposed to perpendicular wind conditions, the vortex in the street canyon is well predicted by 2D simulations (Sini et al., 1996), a two-dimensional study is conducted. In this section, we first describe the three sub-models. Afterwards the coupling strategy is presented.

### CFD model

The CFD simulations are conducted using Ansys-Fluent 12.0 which uses the control volume method (Ansys Inc. 2009). Based on the validation work of Blocken et al. (2009), and Defraeye et al. (2010), steady RANS in combination with the realizable  $k-\epsilon$  turbulence model and Low Reynolds number modeling (LRNM) was selected. Second-order discretization schemes as well as the SIMPLE algorithm for pressure-velocity coupling are employed. Pressure interpolation is second order. At the inlet of the domain, vertical profiles of the mean horizontal wind speed (logarithmic law), turbulent kinetic energy ( $k$ ) and turbulent dissipation rate ( $\epsilon$ ) are imposed representing an atmospheric boundary layer. Symmetry is imposed at the top of the computational domain, which implies that the velocity component normal to the top surface is zero, as are the normal gradients of all other quantities. Zero static pressure is imposed at the domain outlet. The remaining surfaces, i.e. the roofs, the street canyon walls and the ground surface, are modeled as no-slip boundaries with zero roughness. More details can be found in Saneinejad et al. (2011).

A 2D structured grid was constructed based on a grid sensitivity analysis consisting of 16706 control volumes. The  $y^+$  values of the wall-adjacent cells are below one, which is required for boundary-layer modeling with LRNM (Ansys Inc., 2009). Figure 1 presents the geometry of the domain.

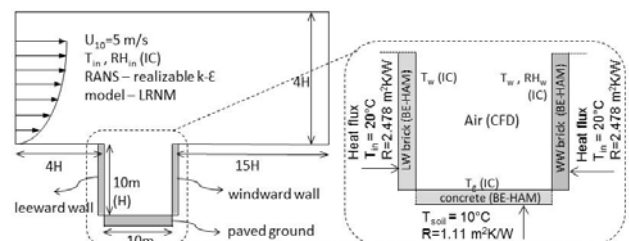


Figure 1. Calculation domain for the coupled model, with close-up view (right) of the street canyon

## BE-HAM model

Drying of the porous material is simulated using a Building Envelope Heat and Moisture (BE-HAM) transport model. This model solves the coupled heat and moisture (vapor and liquid) transport in porous media by means of the finite element method. A detailed description of the basic assumptions and governing equations can be found in Defraeye (2011) and Janssen et al. (2007). Important to note is that latent heat due to vapor diffusion in the material and at the surface is explicitly taken into account in this model.

In this study, the BE-HAM model consists of three separate domains, namely for the windward wall, the leeward wall, and the ground. The windward and leeward walls are 10 m high, built of masonry of 0.09 m thickness insulated on the interior side (thermal resistance of 2.467 m<sup>2</sup>K/W). The indoor temperature is 20°C. The top and bottom surfaces of the brick walls are assumed to be adiabatic and impermeable to moisture. Because of the specific wall construction, i.e. since the insulation material is assumed impermeable to moisture, we can limit the study to the moisture transport in the masonry outer leaf. The material properties for the considered brick can be found in Janssen et al. (2007). The ground is assumed to consist of a 10 cm thick concrete layer over soil. For calculation purposes, we consider a 0.9 m thick soil layer. The soil temperature at 1 m depth is chosen to be 10°C and thermal resistance is 1.11 m<sup>2</sup>K/W. The material properties for the considered concrete can be found in Janssen et al. (2007).

The exterior surfaces are exposed to the following boundary conditions:

$$q_h = CHTC (T_w - T_{ref}) + (L_v + C_v \cdot T_w)q_{c,m,w} + q_{rad}, \quad (1)$$

$$q_m = q_{c,m,v} = CMTC (P_w - P_{ref}) \quad (2)$$

where  $q_h$  (W/m<sup>2</sup>) is the total heat flux,  $q_m$  (kg/m<sup>2</sup>s) is the total mass flux,  $q_{rad}$  (W/m<sup>2</sup>) is the combined short and long wave radiative flux at the wall surface,  $q_{c,m,w}$  (kg/m<sup>2</sup>s) is the convective mass flux,  $T$  (K) is the absolute temperature,  $p$  (Pa) is the vapor pressure,  $C_v$  (J/kg.K) is the specific heat capacity of water vapor,  $L_v$  (J/kg) is the latent heat, and CMTC and CHTC are the convective mass and heat flux coefficients respectively. Subscript  $c$  relates to convective,  $h$  to heat,  $m$  to moisture,  $w$  to (wall) surface values and  $ref$  to values at the reference location.

## RAD model

The radiation model solves the radiative balance, considering the long-wave radiative exchange between windward wall, leeward wall, ground and sky, as well as the incoming shortwave solar radiation. The long-wave radiation flux for a surface  $k$ , ( $Q_{l,k}$  (W)), while taking into account multiple reflections to surface  $k$  from other surfaces  $i$  (where  $i=1,n$ ), is calculated as:

$$Q_{l,k} = A_k \varepsilon_k \sigma \sum_{i=1}^n G_{i,k} (T_k^4 - T_i^4) \quad (3)$$

$$\text{where } G_{i,k} = (I - F_{i,k} \rho_k) F_{i,k} \varepsilon_k \quad (4)$$

where  $i$  is any surface that exchanges long-wave radiation with surface  $k$ ,  $T$  is the absolute temperature (K),  $\sigma$  is the Stefan-Boltzmann constant ( $5.67 \times 10^{-8}$  W/m<sup>2</sup>K<sup>4</sup>),  $\varepsilon$  is the emissivity (here chosen as 1 for sky, and 0.9 for the rest of the surfaces),  $A$  is the surface area (m<sup>2</sup>),  $\rho$  is the reflectivity ( $1-\varepsilon$ ),  $I$  is the identity matrix,  $G_{i,k}$  is the Gebhart between surfaces  $i$  and  $k$ , and  $F_{k,i}$  is the view factor between surfaces  $i$  and  $k$ .

The short-wave radiation flux for surface  $k$  ( $Q_{s,k}$  (W)) including multiple reflections is calculated as:

$$Q_{s,k} = A_k (1 - \alpha_k) I_{0,k} + \sum_{i=1}^n A_i G_{i,k} \alpha_i I_{0,i} \quad (5)$$

where  $G$  is the Gebhart factor as described above,  $I_{0,k}$  is the solar radiation intensity flux for surface  $k$  (W/m<sup>2</sup>) (calculated at  $I_0 \cdot \sin(\gamma)$  where  $I_0$  is the solar radiation intensity flux (W/m<sup>2</sup>) and  $\gamma$  is the angle between the surface and the sun ray), and  $\alpha$  is the surface albedo (here chosen as 0 for sky, 0.4 for leeward and windward wall and 0.1 for ground). For this study, the sky temperature is chosen to be 15°C. The total radiation flux  $q_{rad}$  is calculated as  $(Q_{l,k} + Q_{s,k})/A_k$ .

## Coupling strategy

An efficient coupling strategy has been developed. Since the dominant time-scales in the air domain are much smaller than in the porous domains, we can assume that the air flow quasi immediately accommodates to changes in boundary conditions at the interface. The transport in the porous material is characterized by larger time-scales and hence transient behavior has to be considered. Furthermore, the properties of common porous materials exhibit severe non-linearity, especially those governing moisture transport. Therefore, steady state CFD simulations are conducted for the air domain at every coupling time step, while the BE-HAM simulations are performed transient within this coupling time step: they employ adaptive sub-stepping. The size of the coupling time step ( $\Delta t$ ), governing data exchange between the two models, is determined based on a sensitivity study and is 112 seconds. The diagram below (Figure 2) shows the schematics of the exchange process. The steps included in the coupling can be described as follows:

1. BE-HAM model conducts a transient simulation for a coupling time step of  $\Delta t$  and passes the final surface temperatures to the RAD model. The RAD model calculates the long and short-wave radiative balance at the surfaces and sends back the new radiative heat fluxes to BE-HAM after which a new BE-HAM simulation can be conducted. The BE-HAM and RAD model exchange data (temperature and radiative heat flux) until convergence is reached.
2. The final surface temperatures as well as the moisture contents, calculated using BE-HAM, at the interfaces between the air and porous domains are passed on to CFD and a steady-state CFD simulation is performed.
3. CFD passes CHTC and CMTC values at the air and porous domain interfaces to BE-HAM. These CTCs are calculated from the heat or mass fluxes provided by CFD and a reference temperature or vapor pressure ( $T_{ref}$  or  $P_{ref}$ ) taken at the center of the street canyon.

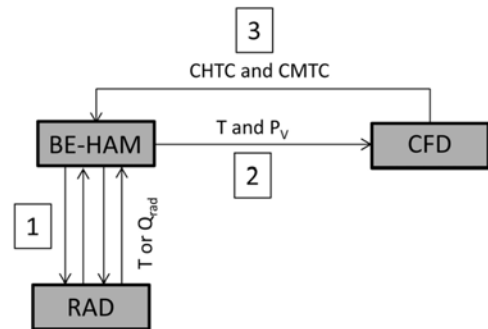


Figure 2. Schematic representation of the coupled model. The exchanged information is labelled in the middle of each arrow. The numbers represent the coupling sequence as described in the text.

From this point onwards, steps 1 to 3 are repeated again until the end of the simulation.

### Example of coupled modeling

The coupled model is used to calculate the temperature and drying rate in the walls and in the air of the street canyon. A square-shaped canyon is chosen as a generic element of the urban canopy. The canyon is 10 m wide and 10 m high. Figure 3 presents simulated results.

This detailed study of the drying of a wet windward wall in a street canyon is able to capture the behavior during two distinct drying phases. During the first drying period, the wall cools down due to the latent heat of evaporation, while, in the second drying period, the cooling effect partially disappears. The cooling of the wall surface leads to an additional decrease of the air temperature in the street canyon. To evaluate the outdoor thermal comfort, the Physiological Equivalent Temperature (PET) was calculated for two pedestrian positions in the street canyon, one exposed to sun and one in the shadow. It was shown that evaporative cooling results in lowering the PET values for both positions. The model shows the potential to accurately model the evaporative cooling effect resulting from drying porous wall surfaces and its influence on the local micro-climate in a street canyon. After full validation, the model will be used to study the evaporative cooling effect for more complex urban geometries and under different boundary conditions.

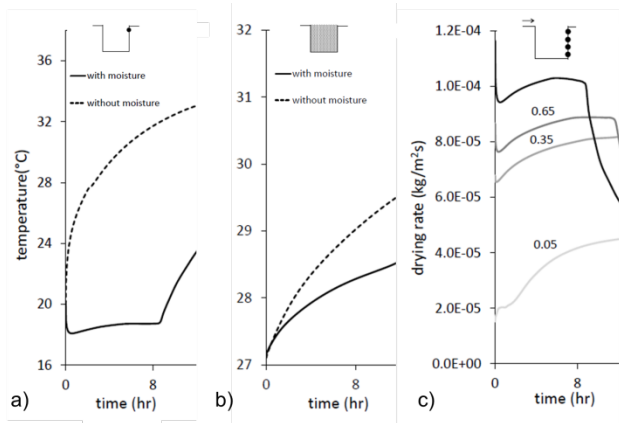


Figure 3. Results of the coupled model for the street canyon exposed to constant boundary conditions over the studied period of 12 hours. (a) surface temperature at position 0.95, with and without initial wetting of the windward canyon wall, (b) air temperature and, (c) mass flow rate at four locations along the height of the windward canyon wall.

### Experimental data for validation of coupled model

The coupled model requires advanced experimental data for full validation. An experiment was designed to provide data with high temporal and spatial resolution in terms of moisture content variations of porous materials exposed to air flow, thus providing data for the coupling between CFD and BE-HAM. Further experiments will involve scaled configurations of street canyon and radiative exchange conditions.

### Description of the wind-tunnel

The wind tunnel, shown in Figure 4, is of open circuit configuration and is made mainly from transparent polymethylmethacrylate (PMMA) while the test section is made from aluminium in order to be transparent to neutron beam. By fan control, various centreline air speeds at the inlet of the channel (10 mm high) can be achieved. After the diffusing section, the air flow passes through a honeycomb and a 2D contraction which provide flow conditioning. The test section has a height-to-width ratio of 7, being the minimum ratio for having a quasi two-dimensional channel flow. For more detailed description about the wind tunnel, refer to Defraeye (2011).

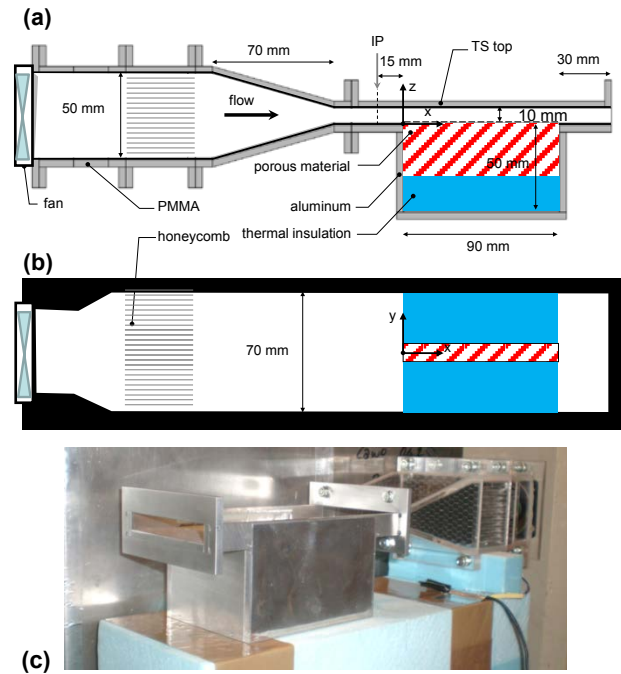


Figure 4. Schematic representation of the micro-wind tunnel, a) side view, b) plan view, c) photo of the micro wind-tunnel in place of the neutron beamline, with test section in aluminium.

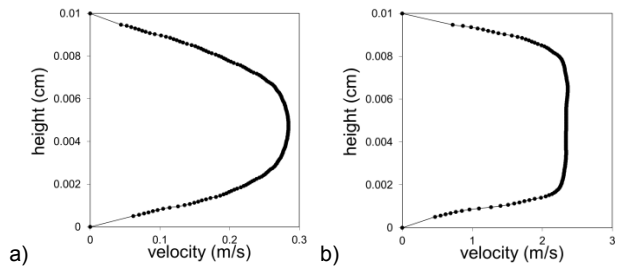


Figure 5 Velocity profile at inlet (IP) at the center of the channel for a) the brick drying experiment, b) the asphalt drying experiment, measured with particle image velocimetry.

### Experimental procedure

The tested samples measure 30 x 89 x 10.3 mm<sup>3</sup> and are made out of clay brick and porous bituminous asphalt. The samples were initially wetted for approximately 1 hour to a moisture content of 120 kg/m<sup>3</sup> for brick and for 8 hours to a moisture content of 40 kg/m<sup>3</sup> for asphalt. The samples were then placed, one after the other, in the center line of the channel of the micro wind tunnel for a duration of 24 hours, exposed to air with speed of approximately 0.28 m/s for brick (Re = 200) and 2.3 m/s for asphalt. Flow conditions are laminar. The neutron images are acquired every 2 minutes. The sample is wrapped tight with aluminum tape all around except the top surface exposed to the air, and is sandwiched between two pieces of 3 cm thick Extruded Polystyrene Insulation (XPS), with thermal conductivity of 0.034 W/mK. This is to minimize drying of the sample through other surfaces and to insure the sample dries mainly from the top.

The detector consisted in a scintillator-CCD camera-system, with a total field of view of 217 x 217 mm<sup>2</sup>. The scintillator converts the neutron signals into visible light photons. The photons are then led via a mirror onto a cooled 16-bit CCD camera (1024 x 1024 pixels). The exposure time is 12 seconds per radiography. Attained spatial resolution is 106 microns. After image processing, the attained moisture content resolution is better than 100 g/m<sup>3</sup>.

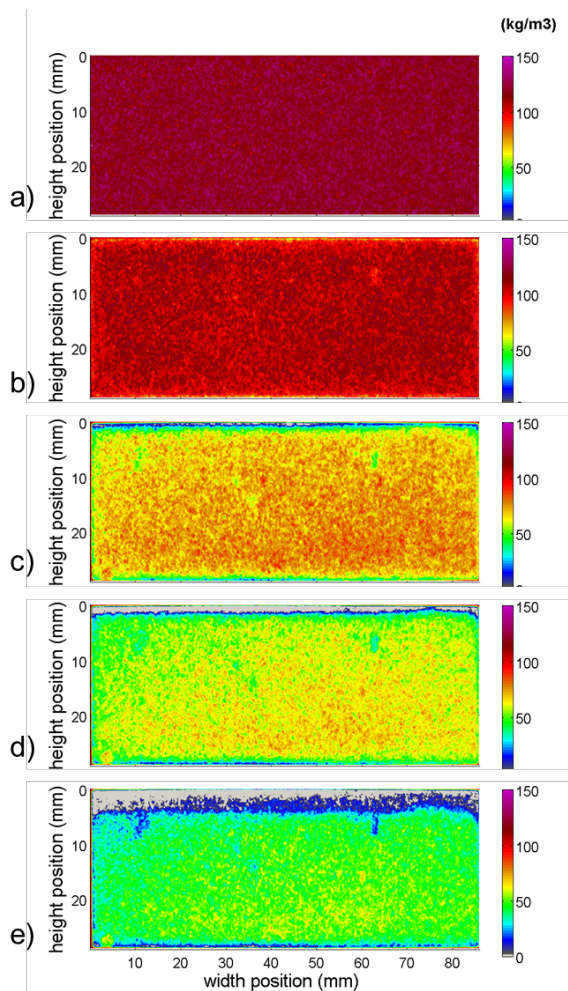


Figure 6. Moisture content distribution in the brick sample, imaged with neutron radiography at: a) initial state, b) state after 1 hour, c) state after 5 hours, d) state after 9 hours and e) state after 21 hours.

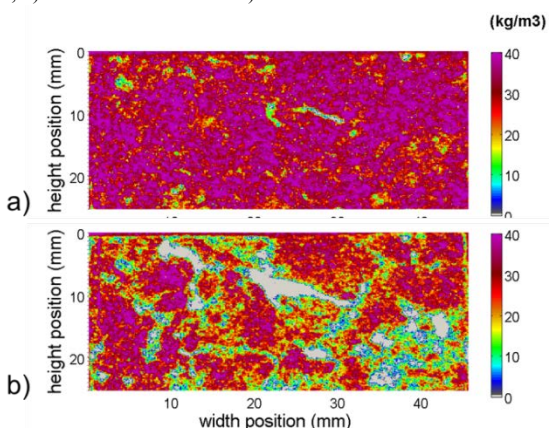


Figure 7. Moisture content distribution in the asphalt sample, imaged with neutron radiography at: a) initial state, b) state after 21 hours.

Preliminary results are shown in Figures 6 and 7. Neutron radiation has a strong interaction with hydrogen which makes neutron radiography an ideal method for measuring the changes in moisture content during the drying of the two porous materials. Brick drying displays clearly the onset of the second drying phase with the appearance of a much dryer layer from Figure 6c onwards. Asphalt, due to its coarse porosity, displays a much more complex drying behaviour, with local drying regions clustering around big pores. Given that the air flow can be fully documented using particle image velocimetry and a high resolution temperature and relative humidity sensor, this

experiment provides all the data required for full validation, i.e. temporal air conditions and moisture content distribution in the materials. This validation work is on-going.

## Conclusion

In this paper, a coupled approach for accurately modeling the effect of evaporative cooling by the drying of porous surfaces in a street canyon, is proposed. The coupled model consists of three sub-models: a Computational Fluid Dynamics (CFD) model which solves the convective heat, air and moisture transport in the air, a Building Envelope Heat and Moisture (BE-HAM) model which solves heat and moisture transport within the porous material, and a radiation model (RAD) which solves the radiative balance at the surfaces, considering the long-wave radiative exchange between the surface and the sky, as well as incoming solar radiation. An example of a coupled calculation is briefly reported.

In addition, as all models need validation to assess reliability, a novel small scaled experimental procedure is presented. Preliminary data demonstrates the richness of the results which is quite promising for the further data analysis and model validation.

## Acknowledgments

Thijs Defraeye is a postdoctoral fellow of the Research Foundation – Flanders (FWO). The support of FWO is gratefully acknowledged. The neutron images were acquired at the Neutron beamline of SINQ, Paul Scherrer Institute, Villigen, Switzerland.

## References

- Ansys Inc. (2009) Ansys Fluent 12.0 User's Guide
- Blocken, B., Defraeye, T., Derome, D., Carmeliet, J., (2009) High-resolution CFD simulations of forced convective heat transfer coefficients at the facade of a low-rise building, *Building and environment* 44:2396-2412
- Defraeye, T., Blocken, B., Carmeliet, J., (2010) CFD analysis of convective heat transfer at the surfaces of a cube immersed in a turbulent boundary layer, *Int. J. Heat Mass Trans.* 53:297–308
- Defraeye, T., (2011) Convective heat and mass transfer at exterior building surfaces, PhD thesis, Katholieke Universiteit Leuven, Belgium
- Janssen, H., Blocken, B., Carmeliet, J., (2007) Conservative modeling of the moisture and heat transfer in building components under atmospheric excitation, *Int. J. Heat Mass Trans.* 50, 1128-1140
- Richards, P.J., Hoxey, R.P., (1993) Appropriate boundary conditions for computational wind engineering models using the k-ε turbulence model, *J. Wind Eng. Ind. Aerodyn.* 46-47:145-153
- Saneinejad, S., Moonen, P., Defraeye, T., Derome, D., Carmeliet, J., (2011) Coupled CFD, radiation and porous media transport model for evaluating evaporative cooling in an urban environment, submitted to *J. Wind Eng. and Industrial Aerodynamics*
- Santamouris, M., (2001) Energy and climate in the urban built environment. James & James
- Sini, J.F., Anquetin, S., Mestayer, P.G., (1996) Pollutant dispersion and thermal effects in urban street canyons, *Atmospheric Environment* 30:2659-2677
- Wieringa, J., (1992) Updating the Davenport roughness classification, *J. Wind Eng. Ind. Aerodyn.* 41-44: 357-368